TRANSONIC AERODYNAMICS IN CONCEPTUAL AIRCRAFT DESIGN

Peter Weiand, B. Eng.
FH Aachen University of Applied Sciences,
Department for Flight Systems, Flight Guidance and Control,
52064 Aachen, Germany

Abstract

The focus of this paper is on methods to solve problems of transonic flow during an aircraft design study. The methods are based on the theory of the infinite shearing wing, refined by understanding of finite wing effects and isobar pattern. The equations required for plan form design and optimization are derived in order to give an aero-structural-design-tool the boundary requirements related to transonic flow. Empirical estimations to link Mach number lift coefficient and thickness are as far as possible avoided. Consequently airfoil data like the pressure distributions as well as the drag and lift divergence Mach numbers and so on are obtained from CFD calculations. The difference of effective sweep in the results of a Vortex Lattice Method and CFD codes are demonstrated on a finite wing as an example. It's shown that the effective sweep angle of a forward swept wing has the tendency to increase depending on the calculation error in contrast to a conventional backward swept wing where the sweep angle decreases. Furthermore a method is demonstrated which allows an easy and fast adaptation of the wing geometry, based on 2D airfoil data in order to achieve a design point with desired sweep and lift distribution. The methods are suited for single finite wings or joint and non-planar wing systems. The setup and grid generation of 2D and 3D models for turbulent CFD analysis at transonic speeds will not be regarded in this paper.

1. INTRODUCTION

1.1. Background

With the respect to the challenges of future economic boundaries new aircraft designs will deal with the optimization of the fundamental aircraft configuration in order to achieve a significant increase in efficiency. Configuration aerodynamics will concentrate on radical new arrangements of wings and stabilizers. The project Advanced Aircraft Configuration is dealing with the design and optimization of new highly non-planar wing systems. Objective is to analyze and adapt new configurations for transport aircrafts with a customized lift distribution and a recognizable reduction of induced drag. Advanced Aircraft Configuration is already working with the Box Wing and the Strut Braced Wing as new concepts which were not realized in the manned transport aviation.

Concept studies have to evaluate new aircraft concepts in order to achieve knowledge of the expected efficiency and handling qualities. Calculation methods used in this manner are related to the resources of the project teams and its manpower. Efficient and capable procedures have to connect the different design tasks.

1.2. Problem

Typical transport aircrafts are flying at transonic speeds. Besides the design aim of reducing induced drag and structural weight the effects of high subsonic flow have to be taken into account in order to achieve a required design point. Therefore drag rise, sweep effects and properties of supercritical airfoils have to be integrated into an aero-structural design tool. To deal with the specialties of non-planar configurations some extensions from the preliminary design phase have to be integrated into the initial sizing phase. The essential achievement is the capability to implement these features on the basis of wing optimization on the level of conceptual design.

1.3. Approach

A short synopsis of compressibility effects will introduce into to system of swept wing. The theory of sweep is derived in more detail on basis of the infinite shearing wing and an extension to finite swept wing. The concept of isobar sweep will be taken into account from thereon. To dimension a finite swept wing with the respect to Mach number section lift coefficient and wing thickness, it will be reduced to a two dimensional problem. Chapter 4 compares different methods of computation and focuses on the effective angle of sweep. The methods are a Vortex Lattice Code on basis of the three-quarter-chord-method, an Euler code and a Navier-Stokes code tailored with a one equation RANS model. Chapter 5 describes a possibility of transforming the wing geometry in terms of adapting the airfoils in the different wing sections. An easy way to scale supercritical Airfoils based on the NASA SC(2)-family gives the chance of utilize a reasonable distribution of camber and twist. Chapter 6 will deliver some useful conclusions to implement the presented procedures into an aircraft design study with priority of configuration aerodynamics.

2. FUNDAMENTALS OF HIGH SUBSONIC AERODYNAMICS

2.1. Compressibility

Up to a Mach number of 0.3 a flow can be considered as incompressible. But beyond that line compressibility changes of more than 5% have to be expected. The first who have tackled this problem were Prandtl and Glauert

with their compressibility correction of the pressure coefficient.

(1) $C_P = \frac{C_{P,IC}}{\sqrt{|1-M_\infty^2|}}$

Equation (1) was derived by linearization of the full potential equation. This procedure is quiet good documented in the works of Schlichting and Truckenbrodt [1] and Anderson [2]. Their ways are slightly different. The derivation should not be repeated here, but it is important to note that the correction factor is obtained by transforming the linearized potential equation and neglecting the transonic region close to M_∞=1. The absolute value of the term under the square root is an extension of the Prandtl-Glauert rule in order to combine it with the Ackeret rule for the supersonic case. The factor in the denominator is sometimes called the Prandtl-Glauert-Ackeret factor and indicated with β.

(2) $\beta = \sqrt{|1 - M_\infty^2|}$

The load coefficient ΔC_P is the vector sum of the pressure coefficient C_P from the top and the bottom panel. The lift coefficient C_l is derived by integrating the load coefficient over the non-dimensional chord of an airfoil. Hence equation (1) can be used to correct the lift coefficient and lift gradient directly. The accuracy of this equation has been slightly improved several times. Considerable are the corrections of Kármán-Tsien and Laitone given with equation (3) and (4).

(3) $C_P = \frac{C_{P,IC}}{\sqrt{1-M_\infty^2}+\left(\frac{M_\infty^2}{1+\sqrt{1-M_\infty^2}}\right)\cdot\frac{C_{P,IC}}{2}}$

(4) $C_P = \frac{C_{P,IC}}{\sqrt{1-M_\infty^2}+\left(M_\infty^2\cdot\left(1+\frac{\kappa-1}{2}\cdot M_\infty^2\right)\cdot\frac{1}{2\cdot\sqrt{1-M_\infty^2}}\right)\cdot C_{P,IC}}$

The κ introduced in equation (4) represents the ratio of the specific heats. But still every correction rule neglects a solution for $M_\infty \approx 1$. In general there are two definitions of the transonic realm. The first is given by the appearance of a mixed flow of subsonic and supersonic velocities. Such a flow is also termed supercritical. For the critical condition the point is considered where the flow reaches the speed of sound. Equation (5) gives the critical pressure coefficient for a given free stream Mach number M_∞.

(5) $C_{P,CR} = -\frac{2}{\kappa\cdot M_\infty^2}\cdot\left[1-\left(\frac{2}{\kappa+1}+\frac{\kappa-1}{\kappa+1}\cdot M_\infty^2\right)^{\frac{\kappa}{\kappa-1}}\right]$

$C_{P,CR}$ indicates the sonic line of a flow field. Equation (5) consists of an isentropic relation and cannot be applied to calculate $C_{P,CR}$ downstream of a shock wave. The critical Mach number M_{CR} can be estimated for an airfoil with given incompressible pressure coefficient $C_{P,IC}$ at the suction peak. Reading the Mach number at the point where the plots of equation (1) and (5) cross each other will give M_{CR}. For the first definition transonic equals with supercritical. But it has one deficit. An airfoil with a blunt leading edge in supersonic flow has a detached shock wave. The flow behind the shock is subsonic and the complete flow is mixed even with large supersonic free stream Mach numbers. The second definition is not as precise as the first for subsonic flow but reliable for supersonic conditions. The transonic realm is simply defined as the Mach number interval, where a prediction of the aerodynamic properties by equation (1) and in edition (3) and (4) is not possible. Never the less the critical Mach number is very practical to clearly divide the transonic region from the compressible subsonic even if compressibility approximations are still precisely.

2.2. Transonic effects on an airfoil

Figure 1 gives the lift and drag coefficients over the Mach number of a DSMA-523a airfoil gained by a CFD analysis with a one equation turbulence model. Here the phenomena drag divergence and shock stall can be observed.

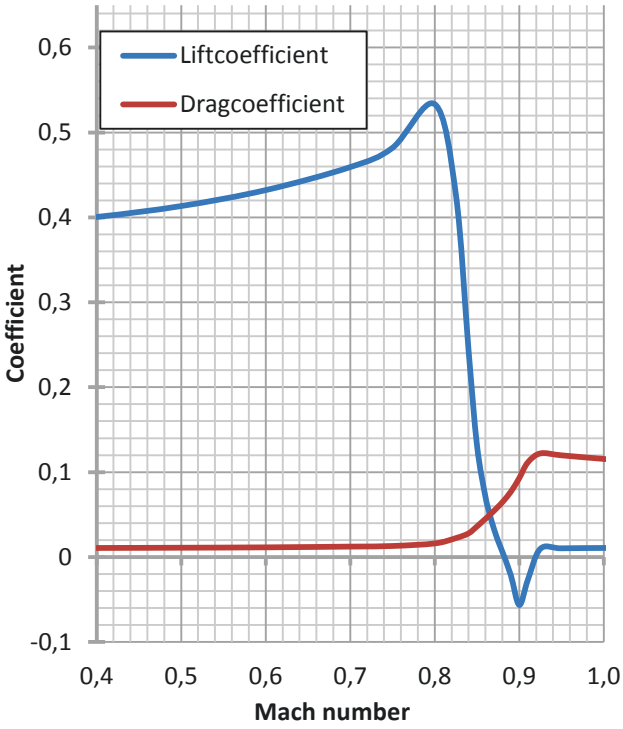

Figure 1 Lift and drag plot of a DSMA-523a

For a constant Reynolds number with increasing Mach number the drag remains steady until an intense increase of pressure drag at a Mach number close to 0.8.

There are three mechanisms which increase the velocity on top of an airfoil. First is the thickness, the second is the angle of attack and last is the camber. Hence the critical Mach number is directly depending on the thickness and lift of an airfoil.

In general the deceleration of a supersonic flow in direction to the trailing edge can happen by isentropic recompression or by a shock. The theory of isentropic deceleration is discussed by Küchemann [3] for shock free airfoils and by Harris [4] for NASA supercritical airfoils.

Wing sections with a moderate nose radius show the maximum velocity shortly after the leading edge. At supercritical conditions the flow will reduce pressure due to expansion waves. Hence the velocity will increase. The expansion waves are now reflected by the sonic line as compression waves. Compression waves are now reflected from the airfoils top as compression waves or in case of a sharp angle of incidence as expansion waves. If the compression waves outbalance the expansion waves the flow will be decelerated smoothly.

In case of the NASA airfoils first an isentropic

recompression occurs followed by a weak shock. The DSMA-523 is a supercritical airfoil based on the NASA SC(2)-series. The possible interval for shock less recompression is very small. Hence most deceleration takes place by a shock. The boundary layer behind the shock becomes thicker. With increasing Mach number the shock walks to the trailing edge and gets stronger. At the point where the pressure gradient between shock wave and trailing edge is to high the flow on the surface turns back and separates. For most airfoils the flow reattaches but the separation produces a strong drag rise.

Drag divergence is mostly defined as the Mach number where the drag gradient $\partial C_d/\partial M$ reaches a value of 0.1. At that point the flow on the lower panel of the airfoil is near to supercritical condition. The result is with increasing Mach number a second shock on the lower airfoil panel will appear. If the flow now separates on booth panels a deflection of the stream downward doesn't proceed. The lift will break down and the point of lift divergence or shock stall is reached. Due to the weaker separation needed for drag rise the drag divergence Mach number M_{DD} is smaller than the lift divergence Mach number M_{LD}. The size of the gap between lift and drag divergence is specified be the present airfoil geometry.

The term M*(L/D) is commonly known as the aerodynamic range coefficient of the Breguet range equation. Regarding the aerodynamic of an airfoil integrated in a finite wing and neglecting the specific fuel consumption and the fuel fraction the highest range would be given at the point of drag divergence. Hence it's understandable that by reaching the drag divergence in one wing section the economic efficiency of an aircraft would decrease rapidly.

In general there are three ways of weakening this transonic effect in terms of configuration aerodynamics. The first is the implementation of a swept leading edge. The second is the integration of supercritical airfoils. Both attempts are shifting the drag rise to higher Mach numbers and therefor increase the aerodynamic range coefficient.

The third method of transonic optimization is the area ruling which is performed for the complete assembly of all components and is not discussed in this paper.

3. SWEPT WINGS

3.1. Infinite shearing wing

The origin of the swept wing is the theory of the infinite shearing wing. By sweeping the leading edge of a wing with infinite span the free stream velocity vector is no longer perpendicular to the lifting surface. The pressure distribution will decrease with the cosine of the sweep angle φ. Hence the pressure and lift coefficient and the complete lift of the wing decrease with the cosine of the sweep angle too. This context is named the cosine rule. This relation was first examined by Jacobs [5] on the basis of comparing two infinite wings, were one is shearing and the others leading edge is perpendicular to the free stream. Equation (6) describes the relation between a swept and straight wing section where booth are parallel to the free stream.

$$(6)\quad \frac{L_{swept}}{L} = \frac{C_{l,swept}}{C_l} = \frac{C_{p,swept}}{C_p} = \frac{\left(\frac{\partial C_l}{\partial \alpha}\right)_{swept}}{2\pi} = \cos\varphi$$

The stagnation condition C_P=1 does not exists on an incompressible pressure distribution for a swept wing section. Hence a pressure plot of an airfoil will reduce according to equation (6) with the cosine of φ. In this connection the lowest pressure coefficient at the suction peak can rise over $C_{P,CR}$. This is the true advantage of a swept wing.

A wing section that has comparable 2D-properties is now required. Therefore the cosine rule is applied to disassemble the velocity vector in two components whereby one is perpendicular and one is parallel to the leading edge. Figure 2 shows the velocity vectors on a shearing wing. The magnitudes of the two vectors are given by equation (7) and (8).

$$(7)\quad v_N = v_\infty \cdot \cos\varphi$$
$$(8)\quad v_T = v_\infty \cdot \sin\varphi$$

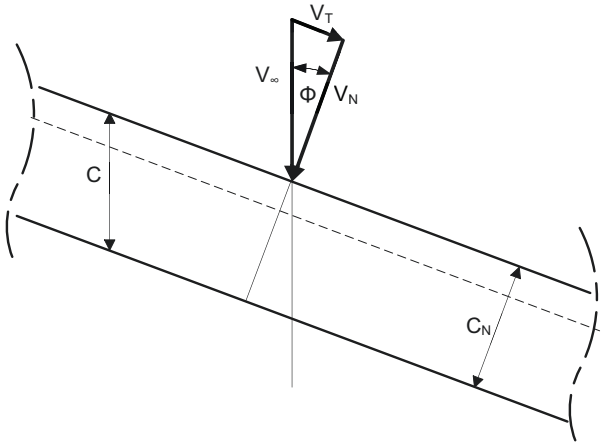

Figure 2 Velocities at an infinite shearing wing

Equation (7) can be extended for the Mach number especially for the cases of the critical condition and drag divergence.

$$(9)\quad \frac{v_N}{v_\infty} = \frac{M_{CR,N}}{M_{CR,\infty}} = \frac{M_{DD,N}}{M_{DD,\infty}} = \cos\varphi$$

Furthermore the chord and thereby the thickness ratio of a wing section perpendicular to the sweep will change.

$$(10)\ t_N = t$$
$$(11)\ c_N = c \cdot cos\varphi$$
$$(12)\ \left(\frac{t}{c}\right)_N = \left(\frac{t}{c}\right) \cdot \frac{1}{cos\varphi}$$

The cosine rule describes the change of lift due to a change of sweep. Now a constant lifting surface with a swept leading edge is under investigation. The overall lift of this section will not change. What changes is the direction in which the aerodynamic properties of a wing section are characterized.

$$(13)\ \frac{\rho}{2} \cdot v_N^2 \cdot S_{ref,N} \cdot C_{L,N} = \frac{\rho}{2} \cdot v_\infty^2 \cdot S_{ref} \cdot C_L$$

The density ρ in equation (13) can be reduced as well as the reference area S_{ref}. The normal velocity component on the left hand side can be expressed by the free stream via equation (7). The result is a relation of the lift coefficients parallel to the flow and perpendicular to the sweep.

$$(14)\ C_{l,N} = C_l \cdot \frac{1}{\cos^2\varphi}$$

This context can be named the cosine square rule. The approach was first performed by Jacobs [5]. The

coefficient $C_{l,N}$ is the required lift from an equivalent 2D section to achieve a desired lift distribution in span direction. Equation (14) can also be used to transform lift coefficient of the airfoils camber at zero angle of attack. To transform the angle of attack the behavior of the lift gradients in the two sections has to be observed.

$$(15)\ \frac{\partial C_{l,N}}{\partial \alpha_N} \cdot \alpha_N = \frac{\partial C_l}{\partial \alpha} \cdot \alpha \cdot \frac{1}{\cos^2 \varphi}$$

The gradient in the normal direction equals to the 2D lift gradient of 2π. The gradient on the right hand side of equation (15) can be expressed by equation (6). The result is a relation between the angle of attack of the 2D equivalent airfoil to the twist distribution normal to the free stream direction.

$$(16)\ \alpha_N = \alpha \cdot \frac{1}{\cos \varphi}$$

The idea is to examine an airfoil in a wind tunnel or a 2D CFD analysis for a new swept wing. The airfoil geometry has to be considered in an effective direction which is perpendicular to the sweep. The thickness of the airfoil has to be larger, as well as the camber and the angle of attack in order to achieve same aerodynamic properties. But the free stream Mach number has to decrease to equal with quasi 2D conditions.

For the derivation of the effective angle of sweep Küchemann [3] provides a more sophisticated approach. In his work he proves by the use of the Euler equation that the effective wing section is perpendicular to the sweep.

3.2. Finite swept wing

In contrast to the infinite shearing wing a finite swept wing consists of three regions where separate sweep effects can be found.

The first is the area close to the wing root. It is majored by the effects of symmetry and fuselage interference. An effective velocity vector has to turn at the center of the wing. Velocities increase and the chord loading of the wing sections around the wing symmetry is shifted backwards.

The second effect is the area of so to speak 2D-flow which can be calculated by the methods derived in subchapter 3.1.

The third is the tip effect at the far outboard wing. Cross flow and pressure compensation between top and bottom force the velocity vectors to the tip edge. Here the chord loading is shifted towards the leading edge.

The expansion of the second area is related to the wings aspect ratio Λ. For wings with an aspect ratio of more than 6 an area with quasi two dimensional properties is visible. At smaller aspect ratios wings are dominated by three dimensional effects. A half wing whereat the whole wing has a Λ=8 is optimal to cut into three sections. Here one quarter of the half span is assigned to the middle effect and one quarter to the tip effect. The remaining 50% of the semi span can be modulated with the shearing wing theory. The percentage of the 3D dominated parts decreases with increasing aspect ratio.

From that point a wing has to be considered as a tapered plan form. Highly tapered wings are quiet common today. Now the fundamental question is which sweep angle between the leading edge and the trailing edge is the representative for the effective aerodynamic sweep of the lifting surface. The isobars on a wing surface are lines of identical pressure and therefor identical velocity. The change of velocity occurs only in the direction perpendicular to the isobars. Figure 3 illustrates the principles of expanding an infinite shearing wing to a finite swept wing. On an ideal and infinite shearing wing the sweep of the leading, quarter chord line, the trailing edge and as a result the isobars is identical.

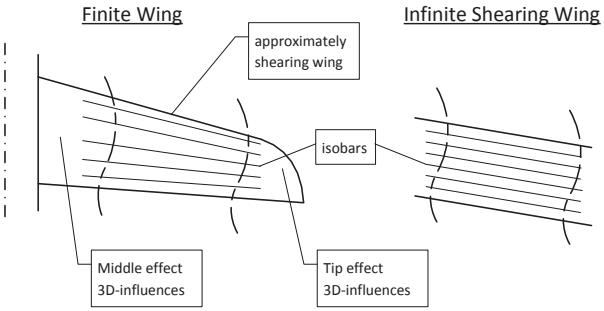

Figure 3 Comparison shearing wing and finite wing

For a finite wing the effective sweep has to be found where most isobars are straight and close to each other. Experiences have shown that the line of recompression on the upper surface is suited best for the effective sweep. Goal of an optimization is now to produce highest possible isobar sweep for a given geometry.

At the wing symmetry the increased chord loading is associated with an unsweeping of the isobars to the wing center due to the turn of the effective velocity direction. At the tip the isobars are turned to the leading edge with the decreased chord loading. This minimizes the efficiency of the wing sweep. Haines [6] gives some basic approaches on treating this problem. Chapter 5 will deal with this theory more precisely.

In order to predict the line of recompression the cosine of the effective sweep angle was often substituted by the following relation:

$$(17)\ \cos \varphi_{eff} = \cos^x \varphi_{25}$$

Equation (17) introduces a new technology factor. With 0.5 Torenbeek [7] gave the first approximation for x. Later the sweep exponent was given the interval from 0.5 to 0.75 by Scholz and Ciornei [8]. This relation would approximate the main isobar sweep behind the 25% chord line what is practical for a conventional aft swept wing. In case of a forward swept wing the value for x has to be larger than 1. The project Advanced-AC conducted further examinations on the isobar pattern related to the wing parameters sweep, aspect ratio and taper ratio. Several wings were analyzed by Ernst [9]. The lift distribution was elliptical. To build the wing shape NACA 65A-airfoils were used. Analysis was carried out by an Euler code. In connection to the work of Weiand [10] it could be proven that the recompression of NACA laminar airfoils could be approximated with the 80% chord line at transonic Mach numbers with an Euler code. This corresponds to the x-value of 0.5 for common wing plan forms. Wings with an aspect ratio of 8, a taper ratio of 0.2 and a quarter chord sweep angle of approx. 33° can be considered as common. For such wings x=0.75 approximates the effective sweep near the 50% chord line. A recompression at 50% chord location is more likely to modern laminar airfoils and supercritical airfoils with a weak lambda shock. For plan forms with more unconventional parameters the substitution and use of a sweep factor on the 25% line is

less functional. Depending on the geometry of the lifting surface values for x can range from 0.35 to 0.8. A reliable prediction of the recompression of a lifting surface without examining the pressure distribution of the airfoils is not possible. In addition the recompression of the 65A-airfoil was calculated with an Euler code at the 80% chord location. Documented wind tunnel results describe the recompression at the 60% of the chord. The primary origin of this difference is the disregard of viscosity by using an Euler code. Subchapter 4.2 will show this more clearly.

Forward swept wings have indeed a higher aerodynamic sweep than a geometric. The recompression was recorded at the same chord locations as the aft swept wings. Horstmann and Streit [11] point out the advantages of forward sweep for a laminar wing with the respect to the location of the recompression zone and the induced downwash. The fundamental disadvantage of a negative sweep angle is the inherent divergent behavior regarding aero elasticity. But for non-planar configurations like Box Wing or Strut Braced Wing aft and forward sweep will appear in a connected wing system.

To summarize there are three sweep angles, which are of vital importance and need to be separated. The leading edge sweep is important to deal with phenomena on the line of highest pressure coefficient like attachment line transition. The quarter chord line is close to the aerodynamic center of the wing sections and in connection with the lift distribution essential for the longitudinal moment around the aerodynamic center of the complete wing. An example for this is a bell curve lift distribution on a swept and tailless flying wing, which makes possible a positive amount of stability. The third one is the line of effective sweep which shouldn't be smaller than the 50% line. Considering the effects described above the isobar pattern will not change the shape of the span loading but its magnitude. The influence of different computational methods on the effective sweep of a given wing plan form will be discussed in chapter 4.

3.3. Considerations for the lift distribution

In general aircraft design studies are aiming for an elliptical lift distribution. This optimizes the coefficient of the induced drag to a near minimum. In this paper the span loading is defined with equation (18) and therefore proportional to the local circulation of a wing section.

$$(18)\ spanloading = C_l \cdot \frac{c}{c_{ave}}$$

Changing the span load from elliptical to triangular shape would optimize the wing bending moment. A very common approach is to derive the complete drag of an aircraft with all subdivided terms.

$$(19)\ D = q_\infty \cdot S_{ref} \cdot C_{D0} + q_\infty \cdot S_{ref} \cdot k \cdot \frac{{C_L}^2}{\pi \cdot \Lambda}$$

Equation (19) gives the aerodynamic drag consisting of the parasite drag and the lift dependent drag. The k-factor is the ratio between the true coefficient of induced drag and the drag coefficient for elliptical lift distribution of a planar wing. S_{ref} represents the reference area and q_∞ the dynamic pressure. The dynamic pressure increases with the square of the Mach number and decreases with the ambient pressure respectively the flight altitude.

$$(20)\ q_\infty = \frac{\rho_\infty}{2} {v_\infty}^2 = \frac{\kappa}{2} \cdot p_\infty \cdot {M_\infty}^2$$

$$(21)\ C_L = \frac{L}{q_\infty \cdot S_{ref}}$$

$$(22)\ \Lambda = \frac{b^2}{S_{ref}}$$

$$(23)\ L = W = m \cdot g$$

By inserting equation (20) to (23) in equation (19) a new relation is obtained.

$$(24)\ D = \frac{\kappa}{2} \cdot p_\infty \cdot {M_\infty}^2 \cdot S_{ref} \cdot C_{D0} + \frac{2 \cdot g^2}{\kappa \cdot \pi} \cdot \frac{1}{p_\infty} \cdot \frac{1}{{M_\infty}^2} \cdot k \cdot \left(\frac{m}{b}\right)^2$$

The parasite drag is proportional to the ambient pressure and the square of Mach number in contrast to the lift dependent drag which is anti-proportional. The objective of configuration aerodynamics is to minimize equation (24). But the lower the wing loading is the larger is the friction drag. Therefor high wing loadings are functional with high subsonic Mach numbers. What actually reduces the lift dependent drag is not a lower wing loading; it is more a higher ratio of wing span over the aircrafts mass. Hence the taper ratio is low and the wing span and the span loading are quiet high. An elliptical lift distribution in connection with a strong taper, results in high local lift coefficients on the outboard wing. The wing section with the highest lift coefficient will be called the critical wing section. This section determines the wing thickness and the stall characteristics. A shifting of the critical wing section towards the wing root would result in a lower critical lift coefficient. As described in subchapter 2.2 for lower lift coefficients the thickness ratio can be increased by keeping the desired M_{CR} or M_{DD} constant. Additionally the critical wing section would be parted from the ailerons and a load shift in case of a stall with the resulting pitch up moment would be reduced. An adapted lift distribution optimizes the wing weight and therefore the induced drag. Furthermore Spohr [12] has proven that the lift distribution of a joint and non-planar wing system for lowest induced drag coefficient is not elliptical in the global coordinate system as well.

4. EFFECTIVE SWEEP DEPENDING ON CALCULATION METHODE

4.1. Vortex Lattice Method

Typically VLM tools split a wing plan form into a structured grid. For each wing section a constant number of elements in chord direction build an elementary wing. Each element has an inbound vortex at its 25% chord line and a control point, were the flow tangency condition is applied. At this point the code assures that the flow doesn't penetrate the element. This approach is also called three quarter chord method. The principles are well documented by Schlichting and Truckenbrodt [1], Anderson [2] and Mason [13]. The properties of a shearing wing are given to each element by a sweep angle of the lifting line. In this case only the Velocity component of equation (7) is at right angles to the inbound vortex line and produces lift with the cross product times the circulation. Equation (25) gives the Kutta-Joukovski theorem for a shearing element in scalar form.

$$(25)\ L_{swept} = \rho \cdot v_\infty \cdot \cos\varphi \cdot \Gamma \cdot dy$$

The width of the trailing lines dy remains invariable and is given by the span fraction of an elementary wing. The magnitude of lift of every element along a wing section is varied by the chord loading of the airfoil family intended to be used.

The sweep of the lifting line of the first element is close to the leading edge angle and analog the angle of the last

lifting line is close to the trailing edge. The average sweep angle of a wing section is at the half chord line. This is an inherent value given by the vortex lattice method.

The accuracy of such methods is limited in the transonic region by two major factors. The chord loading of an elementary wing has at the position of the shock wave a strong nonlinear development. The true chord loading of an airfoil changes with Mach number, Reynolds number and has to fit to the desired effective sweep angle. Errors in the prediction of ΔC_P affect the pitch moment of the wing section and moreover the complete pitch moment around the aerodynamic center.

The second factor is the usage of the Prandtl-Glauert-Ackeret rule. As given with equation (2) the factor is also used to transform a wing plan form from a given Mach number to incompressible conditions in order to solve the design task with a vortex lattice.

$$(26)\ \Lambda_{IC} = \frac{\Lambda}{\beta}$$

$$(27)\ \cot\varphi_{IC} = \frac{\cot\varphi}{\beta}$$

Equation (26) and (27) give the transformation of aspect ratio and geometric sweep. As discussed in chapter 2 compressibility corrections show an increasing failure by entering the transonic area.

4.2. Computational Fluid Dynamics

In terms of conceptual aircraft design computational fluid dynamics can be separated into old codes using the small perturbation theory like TS Foil, more sophisticated codes like Euler solvers and high fidelity Reynolds-Averaged-Navier-Stokes solvers. RANS solutions are typically produced by the use of a one-equation or a two-equation turbulence model. Differences between a standard wall function and an enhanced wall function have to be considered. Small perturbation equations and Euler equations are neglecting viscosity.

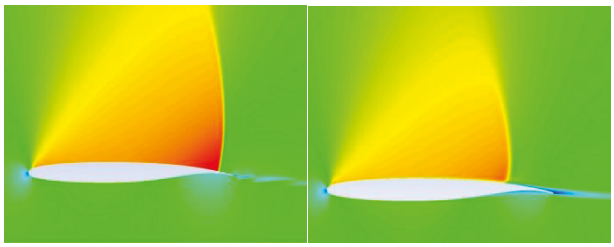

Figure 4 Comparison of Euler and RANS on airfoil

The left picture of Figure 4 shows the Mach number plot of an Euler solution around an 8% supercritical airfoil. The right picture shows the corresponding RANS Solution. The flow condition is beyond drag divergence. The shock line of the RANS solution is recognizable earlier. A turbulent boundary layer enforces a deceleration by a shock earlier than the frictionless solution. The Mach number before the shock is lower and the pressure gradient to the trailing edge is smaller. By neglecting viscosity the drag divergence Mach number is shifted to lower Mach numbers. TS Foil is an open source code with a good comparability to an Euler code. It is possible to calculate the lift coefficient at drag rise correctly. But with a far too low drag divergence Mach number. In order to predict pressure distribution and transonic effect correctly a RANS solution is required.

Figure 5 shows the distribution of the pressure coefficients on a transonic wing at M_∞=0.85. The wing sections base on the NASA SC(2)-series. Left side shows the Euler solution. The right side was calculated by a RANS approach with a one equation turbulence model. The isobars are not optimized until now. As expected the shock line of the Euler solution is farer to the trailing edge. Hence the effective sweep of the isobars is smaller Than the RANS solution. In this connection the left picture shows a wing beyond drag rise. The design point is given by C_L=0.5 at M_∞=0.85.

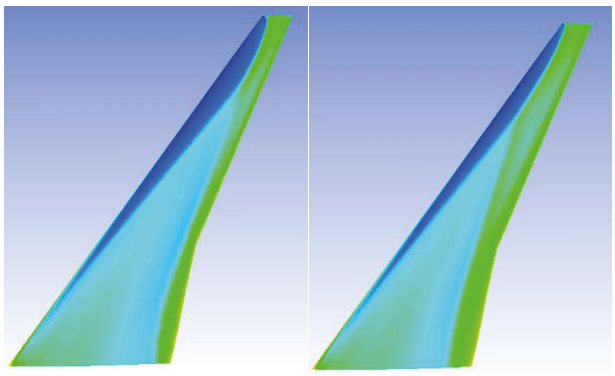

Figure 5 Comparison of Euler and RANS on finite wing

Figure 6 shows the span loading of the three calculation methods. The blue line is the design span loading from the VLM tool. The VLM solution is setup with an effective sweep at the half chord line. Due to the inconstant chord loadings on the quasi shearing wing an unsweeping of the isobars is recognized which has to be treated later. The span wise lift distribution of the RANS calculation is in fact elliptical but because of reduced effective sweep the section values are higher than the design values.

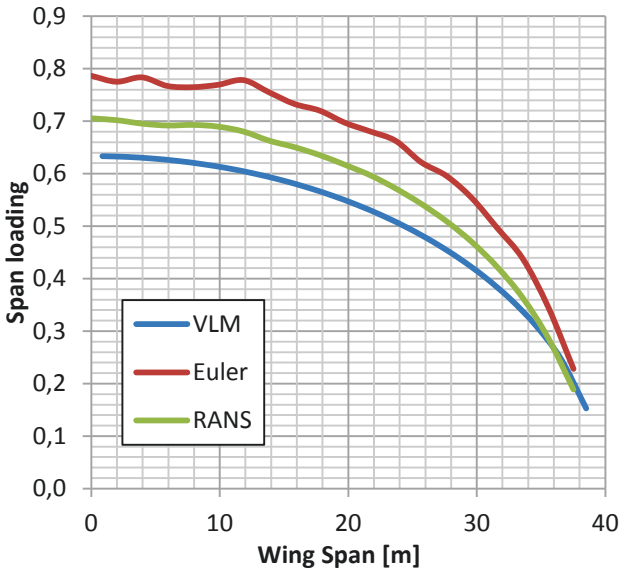

Figure 6 Calculated span loading by different methods

The effective sweep of the Euler calculation is slightly smaller than the trailing edge. Hence the span loading has the greatest failure.

Advanced-ACs first analysis of a non-planar configuration was carried out by Schirra [14] on a Stagger Wing. A stagger wing is an unconnected non-planar wing system

consisting of a forward wing with positive sweep and a rearward wing with a negative sweep. The lift share of booth wings should be equal for this model. The twist distribution was calculated by VLM code LamDes and a validating calculation was carried out by the use of an Euler code. Figure 7 shows the resulting isobar pattern. As discussed above a higher chord loading on the upper side is obtained than predicted by the VLM tool. For the conventional aft swept wing the effective sweep decreases resulting in an increase of effective Mach number and section lift.

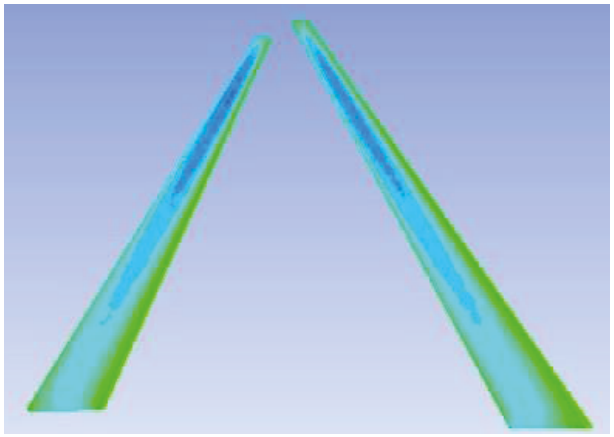

Figure 7 Pressure plot of a stagger wing by Schirra [14]

In contrast to that the effective sweep of the forward swept wing increases which reduces the section C_l of the rear wing. Due to the higher lift of the front wing a stronger induced downwash reduces the section lift of the second wing even more. But the additional lift by means of compressibility influence is larger than the loss on the rear wing by compressibility and downwash. The calculated lift coefficient is slightly higher than the design C_L. But considering the longitudinal moment the error in calculation of booth wings enforces a moderate pitch up moment around the aerodynamic center. This behavior can be expected on a box wing by increasing the flight Mach number over the design cruise speed.

5. WING SECTION DESIGN

5.1. Supercritical Airfoils

The objective of supercritical airfoils is to increase the gap between M_{CR} and M_{DD}. The design of these airfoils is complex and based on computational optimization algorithm. The most comprehensive open source airfoil series of this kind is the NASA SC(2) family. Many airfoil coordinates with different design lift coefficients and thickness ratios are published. Furthermore Harris [4] gives a very good documentation on the design guidelines of NASA's supercritical airfoils and required flow properties for the effective use at transonic velocities. The design point is set at the drag divergence Mach number. Hence the design lift coefficient given in the airfoil label is only available at M_{DD}. The three basic design guidelines will now be repeated in order to outline the groundwork for intermediate airfoils with varying camber and thickness ratios.

The first design guideline is a subsonic pressure plateau at the top of the airfoil below the design point. This is a subcritical condition and actually an off design point. Second guideline is to obtain a limited gradient of pressure recovery on the top to prevent flow separation. Therefore a pressure coefficient close to zero at the trailing edge is desirable. Parallel velocity vector from the bottom and top panel are suitable. Hence the curvature of the two panels has to be parallel. Building a razor sharp trailing edge is not functional. Therefor a blunt trailing edge is introduced with a thickness just a little below the thickness of the boundary layer at 100% of the chord. The third is a sufficient rear loading to insure a large lift coefficient at zero angle of attack. For this purpose the rear bottom panel is strongly cambered. In connection to that an aft acceleration appears behind the shock.

The maximum thickness extends from 34% to 37% of the chord. Up to this chord position the airfoil is symmetrical. At 38% a positive camber is introduced. At 40% the crest of the top panel is reached. If a supersonic flow extends over this chord location an expansion flow occurs and the strength of the shock terminating the supersonic region increases rapidly. The airfoils feature the equal thickness distributions along the chord for same thickness ratio, but varying camber. This gives the opportunity to scale thickness and camber lines separately to get an infinite number of intermediate airfoils without braking with the design guidelines.

Figure 8 shows the Mach number distribution of a 9% thick supercritical airfoil at M_∞=0.75 and a Reynolds number of 35 Mio. The results were calculated by a RANS approach. The flow conditions are marking the design point shortly before the drag rise. The transition from a laminar to a turbulent boundary layer is finished at approx. 3% of the chord which is still in the area of the nose radius. The maximum velocity and isentropic recompression occurs at a completely turbulent boundary layer. The thickening of the boundary layer behind the shock is clearly recognizable as well as the aft acceleration. Here the velocity increases slightly over the speed of sound but decelerates with an isentropic recompression. A shock at that location would increase the pressure gradient over the limits and violate the second design guideline. Considering the requirements for grid generation in order to carry out a RANS calculation the Y^+-values will surely decrease behind the lambda shock. But as soon as the aft acceleration happen the Y^+-values will increase again and not violate the requirements of a standard wall function. This is different to the behavior of the boundary layer on the bottom panel. The strong camber at the tail increases the pressure and therefor decelerates the flow very strongly. The wall-Y^+-values usually tend to fall into the buffer layer in connection with a standard wall function.

Figure 8 Distribution of the Mach number around a 9% supercritical airfoil

The strong similarities of the SC(2)-family not only allow an interpolation of the airfoils thickness. Experiences have shown that an interpolation of the camber line of two airfoils with equal thickness ratio deliver reliable airfoil coordinates. For this purpose four airfoils stretch out a field in which the interpolation will be conducted. Two airfoils have a large thickness ratio in contrast to the other two, which are slender. On of each has a strong camber line whereby the other two have a smaller C_{l0}.

Used were the airfoils SC(2)-0710 and SC(2)-0706 with strong camber and the airfoils SC(2)-0410 SC(2)-0410 with low camber. The thickness ratio has the interval from 6% to 10 %. Figure 9 illustrates the idea of intermediate airfoils.

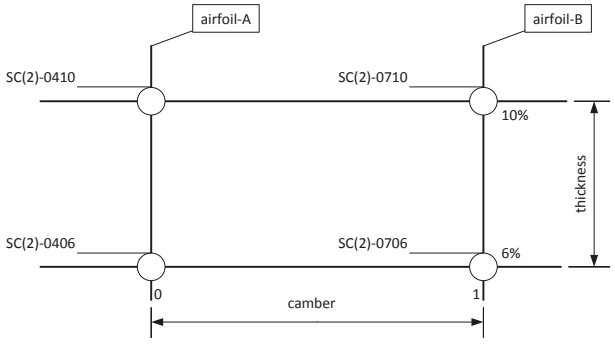

Figure 9 Principle of airfoil interpolation

The first step is to interpolate the airfoils A and B on the desired thickness to chord ratio. Airfoil B has the highest lift coefficient at zero angle of attack. It will be integrated in the critical wing section. The crest of the upper contour will walk towards the leading edge with increasing angle of attack. Thereby the danger of expansion flow and strong shock waves rises. The airfoil designated for the critical wing section should be integrated with an angle of attack close to zero. The thickness of the wing will be determined by the drag rise characteristics of the critical section. Decisive factors are the maximum wing loading at the beginning of the cruise flight and an additional load factor required for maneuvering. Normally a Δn=1.3 is required for cruise speed without significant changes in attitude and stability of flight. Analog the A-airfoil is integrated in the wing section with the lowest camber. The two airfoils have to be pre-scaled to the corresponding wing section. Afterwards a shape function is applied running in the interval form 0 to 1. This function considers the pressure distribution over the chord in span direction. Airfoils interpolated in this manner meet the design guidelines discussed above.

5.2. Transformation of Wing Sections

In order to obtain a 3D geometry of a wing suitable for a numerical calculation in this early stage of design, the wing sections will be transformed into an effective direction. One requirement for this procedure is the implementation in a programming environment like Excel or MatLab. Lifting surfaces are normally defined by at least four breakpoints for the starboard side. By appearance of a kink in leading and trailing edge the number can increase up to six. Such a plan form including a distribution of twist and camber has to be the result of an aero-structural design tool. The fundamental idea is to turn all given wing sections on their aerodynamic center perpendicular to the design angle of sweep. The aerodynamic center will be close to the quarter chord line. The effective sweep should be parallel to the half chord line. A straight connection between the breakpoints is required for this method. In the following example a positive swept wing with a trailing edge kink will be transformed. The wing has in inboard part from the root to the kink which sweep angles are expressed by the index I. The base wing from the kink to the tip carries the index II. Five breakpoints are given with the indexes ‘root,LE’, ‘root,TE’, ‘kink,TE’, ‘tip,LE’ and ‘tip,TE’. Considering the symmetry effects at the inboard wing the effective direction of sweep is curved to the symmetry plane. Now a distribution of the local sweep angle is determined. On the inboard wing the sweep has to be guided to the symmetry plane. Equation (28) gives the sweep of the airfoil sections on the inboard wing.

$$(28)\ \hat{\varphi}_I(y) = \hat{\varphi}_{II} \cdot \left(1 - \left(\frac{y\prime_{kink} - y}{y'_{kink} - y_{fus}}\right)^e\right)$$

The span-coordinate y'_{kink} describes the wing section that ends on the trailing edge kink. Normally this section has to be interpolated. Here it is used to part the inboard from the base wing. The value y_{fus} is the fuselage radius which is zero for this example. The exponent e gives the opportunity to morph the curve with respect to the aspect ratio and the span fraction of the inboard wing.

$$(29)\ \hat{\varphi}_{II} = \varphi_{II,eff}$$

Next step is to calculate the sweep angles of leading edge and trailing edge from the breakpoints. Resulting in the kink there are two trailing edge angles.

$$(30)\ \varphi_{LE} = arctan\left(\frac{x_{tip,LE} - x_{root,LE}}{y_{tip} - y_{root}}\right)$$
$$(31)\ \varphi_{TE,I} = arctan\left(\frac{x_{kink,TE} - x_{root,TE}}{y_{kink} - y_{root}}\right)$$
$$(32)\ \varphi_{TE,II} = arctan\left(\frac{x_{tip,TE} - x_{kink,TE}}{y_{tip} - y_{kink}}\right)$$

The next set of equations gives the corresponding x-coordinate to every span-location y on the edges.

$$(33)\ x_{LE}(y) = tan\varphi_{LE} \cdot (y - y_{root}) + x_{root,LE}$$
$$(34)\ x_{TE,I}(y) = tan\varphi_{TE,I} \cdot (y - y_{root}) + x_{root,TE}$$
$$(35)\ x_{TE,I}(y) = tan\varphi_{TE,II} \cdot (y - y_{kink}) + x_{kink,TE}$$

The local chord length for a straight section is given by Equation (36). With equation (37) to (39) the coordinates on the 25%-line are given including the sweep angles of the lines.

$$(36)\ c(y) = x_{TE}(y) - x_{LE}(y)$$
$$(37)\ x_{25}(y) = x_{LE}(y) + 0.25 \cdot c(y)$$
$$(38)\ \varphi_{25,I} = arctan\left(\frac{x_{25}(y_{root}) - x_{25}(y_{kink})}{y_{root} - y_{kink}}\right)$$
$$(39)\ \varphi_{25,II} = arctan\left(\frac{x_{25}(y_{kink}) - x_{25}(y_{tip})}{y_{kink} - y_{tip}}\right)$$

The next set of equations gives the leading edge coordinates of the added wing section leading to the trailing edge kink normal to the effective sweep.

$$(40)\ y'_{kink,LE} = \frac{tan\varphi_{LE} \cdot y_{root} - x_{root,LE} + x_{kink,TE} + \frac{y_{kink}}{tan\hat{\varphi}}}{\frac{1}{tan\hat{\varphi}} + tan\varphi_{LE}}$$
$$(41)\ x'_{kink,LE} = tan\varphi_{LE} \cdot \left(y'_{kink,LE} - y_{root}\right) + x_{root,LE}$$

The supporting point for every wing section is given by a triple of parameters. All transformed properties carry a circumflex accent. The first is the span location of the wing

section in y-direction. The second is the x-coordinate to the point on which the section is turned.

$$(42)\ \hat{x} = x_{LE} + c_{AC} \cdot c(y)$$

The third parameter is the local angle of sweep. This was already given by equation (28) and (29). With this triple the new leading edge coordinates can be calculated.

$$(43)\ y_{LE}(\hat{x},\hat{y}) = \frac{tan\varphi_{LE} \cdot y_{root} - x_{root,LE} + \hat{x} + \frac{\hat{y}}{tan\tilde{\varphi}}}{\frac{1}{tan\tilde{\varphi}} + tan\varphi_{LE}}$$

$$(44)\ x_{LE}(\hat{x},\hat{y}) = tan\varphi_{LE} \cdot (y_{LE} - y_{root}) + x_{root,LE}$$

The next step is to calculate the trailing edge coordinates of the turned wing sections.

$$(45)\ y_{TE,I} = \frac{tan\varphi_{TE,I} \cdot y_{root} - x_{root,TE} + \hat{x} + \frac{\hat{y}}{tan\tilde{\varphi}}}{\frac{1}{tan\tilde{\varphi}} + tan\varphi_{TE,I}}$$

$$(46)\ y_{TE,II} = \frac{tan\varphi_{TE,II} \cdot y_{kink} - x_{kink,TE} + \hat{x} + \frac{\hat{y}}{tan\tilde{\varphi}}}{\frac{1}{tan\tilde{\varphi}} + tan\varphi_{TE,II}}$$

$$(47)\ x_{TE,I}(\hat{x},\hat{y}) = tan\varphi_{TE,I} \cdot (y_{TE,I} - y_{root}) + x_{root,TE}$$

$$(48)\ x_{TE,II}(\hat{x},\hat{y}) = tan\varphi_{TE,II} \cdot (y_{TE,II} - y_{kink}) + x_{kink,TE}$$

If a coordinate y_{LE} is smaller than the span location calculated with equation (40), then equations (45) and (47) have to be used for the trailing edge on the inboard wing. The y-coordinate of equation (40) has to be taken into account due to the fact that some y_{LE} values are larger than the breakpoint y_{kink} but the trailing edge coordinates of the turned section still ends on the inboard wing.

$$(49)\ c = \sqrt{(y_{LE} - y_{TE})^2 + (x_{LE} - x_{TE})^2}$$

The chord length can also be transformed by equation (11) excluding the area around the kink. For a programming attempt equation (49) should be preferred. Figure 10 shows a wing geometry transformed by the measures described above.

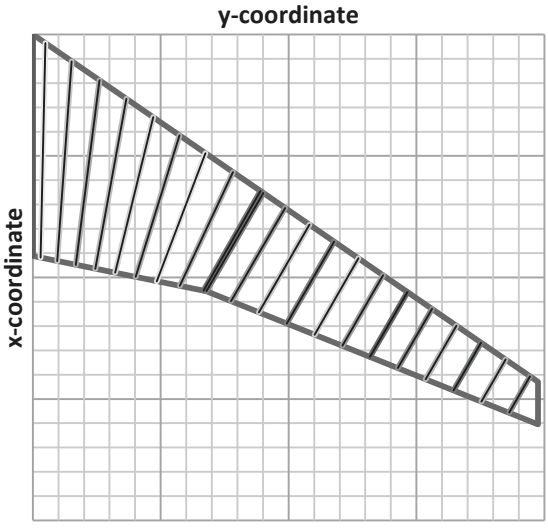

Figure 10 Plot of the transformed wing section geometry

Now every wing section is given by a location of the leading edge, an orientation in the yx-plane and a chord length. The corresponding aerodynamic properties for the transformed geometry are calculated by the use of the equations presented in subchapter 3.1. The transformed angle of attack completes the required orientation.

The geometry given in Figure 10 allows the construction of a wing shape with airfoils that are analyses in a 2D-environment at the effective Mach number. For the specific case of Figure 10 the requirements are an aerodynamic center at 25% of the chord and an effective sweep at 50% of the chord. The combination of high fidelity aerodynamic and structural analysis via this geometry is a possible option.

5.3. Adapted Airfoil Geometry

The final part is to integrate airfoils into the plan form in order to create a 3D-model of the wing. The twist distribution of a lifting surface usually consists of the angle of attack and the angle of induced downwash at the wing. Equation (51) shows the integral equation of Ludwig Prandtl for the simple lifting line theory. The first two summands yield the angle of attack depending on the local circulation and local camber. Here the second term is the angle for zero lift.

$$(50)\ \alpha_{geo}(\hat{y}) = \frac{\Gamma(\hat{y})}{\pi \cdot v_\infty \cdot c(\hat{y})} + \propto_{l0} + \frac{1}{4 \cdot \pi \cdot v_\infty} \cdot \int_{-b/2}^{b/2} \frac{\left(d\Gamma/dy\right)dy}{\hat{y} - y}$$

The first term giving the angle of attack for a flat plate is now called the aerodynamic angle of attack. As a result of a VLM or Panel code equation (50) can be simplified to equation (51) for a wing section.

$$(51)\ \alpha_{geo}(\hat{y}) = \alpha_{aero}(\hat{y}) + \propto_{l0} + \alpha_{ind}(\hat{y})$$

This formulation is valid for the free stream direction, as well as for the transformed wing sections. Twist tables from a design tool are given by the geometric twist or the aerodynamic twist. The aerodynamic twist is simply the distribution of induced angle of attack given by the last term of equation (50). In this case the airfoils can be chosen freely in connection with the table of the C_l over the span. On the other hand the VLM tool LamDes gives geometric twist according to equation (50) or rather (51) with a distribution of the wing sections camber. By knowing the lift coefficients at zero angle of attack and the lift slope the geometric twist can easily be rearranged. Consider that all aerodynamic parameters in equation (52) have to be predicted or calculated at the actual effective Mach number.

$$(52)\ \alpha_{geo,new}(\hat{y}) = \alpha_{geo,VLM}(\hat{y}) + \frac{C_{l0,VLM} - C_{l0,new}}{\left(\frac{\partial C_l}{\partial \alpha}\right)_{new}}$$

The use of the Prandtl-Glauert-rule has shown to be unreliable for $M_\infty \approx 0.85$ and $M_{eff} \approx 0.75$. Especially the factor β in equation (2) shows differences between corrections of C_l and $\partial C_l / \partial \alpha$.

To insure a most accurate sweep of the isobars with the respect to the design sweep a sophisticated distribution of camber is required. A very good introduction into the shaping of isobar pattern is given by Haines [6]. His methods involve changes in camber along the span and thickness along the chord. Recalling the complexity of supercritical airfoils discussed in subchapter 5.1 the only degrees of freedom in this design phase are the zero lift coefficient and the angle of attack.

The shock sweep is given by the recompression of the critical wing section. Airfoils on a base wing with characteristics of a shearing wing have to fulfill the similar recompression location. By decreasing the camber towards the inboard wing a lower pressure recovery is required. Hence isobars tend to the trailing edge. Consequence is an unsweeping of the isobars on the

shearing wing due to the decrease of sections C_l and C_{l0}. Reconsidering the ratio between camber and angle of attack adapts the pressure distribution for constant section C_l. By increasing the angle of attack, the crest of the top panel goes forward and the chord loading decreases. The opposite happens by increasing the camber and decreasing the angle of attack for a given C_l. As mentioned in subchapter 5.1 at least two wing sections are needed to give a reasonable camber distribution via a shape function. The critical section assesses and dimensions the wing. Two sections separate the quasi 2D-wing from the 3D-affected regions. The tip and the root airfoil close the wing shape. The construction of the tip weather it is finished with a winglet or Küchemann-tip can now be considered. The isobars on the three mid wing sections can be predicted very well by 2D-calculations. Root and tip are still construction areas for approximation methods like used by Haines [6]. In the first attempt the shape function for the four segments between the five breakpoints can be linear.

6. CONCLUSIONS

6.1. Plan form design and optimization

An aero-structural-design-tool will estimate the wing thickness by the means of tank volume, stresses of the main spars and lift distribution for lowest weight and induced drag. With the equations given in chapter 3 as well as a good collection of airfoil data, transonic requirements can be integrated into the optimization procedure. CFD results are an important basis for a correct estimation of the transonic effects limiting the plan form optimization. Even for non-planar configurations the conceptual design can fully base on two dimensional airfoil analysis. This is a remarkable fact. But at least with passing the critical Mach number viscosity cannot be neglected in a CFD calculation. Never the less an accurate grid equipped with a blunt trailing edge can be generated with less than 100,000 elements for high Reynolds numbers. Today's personal computer reached a number of eight cores per workstation. Obtaining the results for the flow condition shock stall can take more than one hour by the use of a coupled solver. Flow conditions less complicated demand less than 60 minutes. This increase in computational power is remarkable. Final step is to build a digital 3D-model with the methods discussed before on basis of the plan form breakpoints and the design lift distribution. Experiences have shown that this procedure takes approx. one week for a simple wing with not more than 20 sections. A highly non planar wing system will take more time depending on the number of sections and the complexity of the wing joint.

6.2. Evaluating calculation

To complete a design loop verification has to be performed. An aerodynamic evaluation in this manner can only be carried out by a three dimensional Navier-Stokes method. This calculation is actually the killer criteria for a project team weather it will design for transonic speeds or not. Grid generation for 3D analysis with the respect to boundary layer influence is difficult, time consuming and requires a more sophisticated calculation system. The computation time increases with the higher dimension and the larger number of elements. Results of finite wings like presented in Figure 5 easily need about a 150 times more elements than an airfoil analysis. For non-planar configurations with joint wings and more than one leading and trailing edge which have to be refined, this factor is even higher.

A draft wing in this stage is not optimized for pressure and wave drag. That is a complex three dimensional iteration process which is carried out during the second phase the preliminary design. At this stage the model fulfills a design lift distribution, the linked downwash and good assessment of the longitudinal moment. These results are satisfactory in order to assess the glide number and stability as the major flight physical parameters in order perform a concept study.

LIST OF REFERENCES

[1] SCHLICHTING, Herman, TRUCKENBRODT, Erich A.: Aerodynamik des Flugzeuges Band 1+2. Berlin, Heidelberg : Springer-Verlag, 2001

[2] ANDERSON, J. D.: Fundamentals of Aerodynamics. New York : McGraw-Hill, 1991

[3] KÜCHEMANN, Dietrich: The Aerodynamic Design of Aircraft. Pergamon Press : Oxford, 1978

[4] HARRIS, Charles D.: NASA Supercritical Airfoils. Hampton : NASA Technical paper 2969, 1990

[5] JACOBS, W.: Experimentelle Untersuchungen am schiebenden Flügel. Springer-Verlag, Ingenieur-Archive p418-426, 1952

[6] HAINES, Arthur Barry: Wing Section Design for Swept-Back Wings at Transonic Speeds. Journal Of The Royal Aeronautical Society: Vol. 61 p238-244, 1957

[7] TORENBEEK, Egbert: Synthesis of Subsonic Airplane Design. Delft: University Press, 1979

[8] SCHOLZ, D., CIORNEI, S.: Mach number, Relative Thickness, Sweep and Lift Coefficient of the Wing – An Empirical Investigation of Parameters and Equations. Hamburg: HAW Hamburg University of Applied Sciences, DLRK-Paper, 2005

[9] ERNST, Konstantin: Validierung der Transformations-gleichung für den gepfeilten Flügel endlicher Breite. Aachen: FH-Aachen University of Applied Sciences, 2012

[10] WEIAND, Peter: Aerodynamischer Flügelentwurf für einen Megaliner im Reiseflug. Aachen: FH-Aachen University of Applied Sciences, 2012

[11] HORSTMANN, K. H., STREIT, T.: Aerodynamic Wing Design for Transport Aircraft – Today. Braunschweig: DLR, Institut für Aerodynamik und Strömungstechnik, 2009

[12] SPOHR, Alexander: Konzeptioneller Entwurf für eine Box Wing Konfiguration unter Verwendung eines Wirbelgitterverfahrens. FH-Aachen University of Applied Sciences, DLRK-Paper, 2012
http://www.dglr.de/publikationen/2012/281600.pdf

[13] MASON, William H., Applied Computational Aerodynamics. Blacksburg: Virginia Polytechnic Institute and State University, 1998.
http://www.dept.aoe.vt.edu/~mason/Mason_f/CAtxtTop.html

[14] SCHIRRA, Julian: Aspects of a Conceptional Aerodynamic Wing Design for an Advanced Aircraft Configuration. Aachen: FH-Aachen University of Applied Sciences, 2011